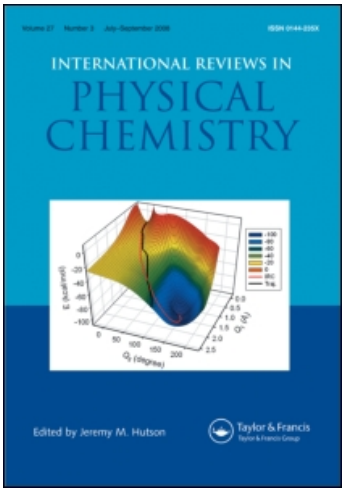

International Reviews in Physical Chemistry
Publication details, including instructions for authors and subscription information:
http://www.informaworld.com/smpp/title~content=t713724383

Permanent electric dipole moments of metal containing molecules

Timothy C. Steimle[a]
[a] Department of Chemistry and Biochemistry, Arizona State University, Tempe, AZ, USA

Online publication date: 26 November 2010

To cite this Article Steimle, Timothy C.(2000) 'Permanent electric dipole moments of metal containing molecules', International Reviews in Physical Chemistry, 19: 3, 455 — 477
To link to this Article: DOI: 10.1080/01442350050034199
URL: http://dx.doi.org/10.1080/01442350050034199

INT. REVIEWS IN PHYSICAL CHEMISTRY, 2000, VOL. 19, NO. 3, 455–477

Permanent electric dipole moments of metal containing molecules

TIMOTHY C. STEIMLE†
Department of Chemistry and Biochemistry, Arizona State University, Tempe, AZ 85287-1604, USA

A summary of the current status of experimentally derived values of the permanent electric dipole moment, μ, for the 3s, 4s, 5s, and 6s series of transient metal containing molecules is given. The experimental methods employed are described with particular emphasis placed upon optical Stark measurements of supersonic molecular beam samples. The complications associated with the analysis of optical Stark spectra of open shell polyatomic metal containing radicals are addressed. An assessment of the applicability of simple molecular orbital correlation diagrams to predict trends in measured values of μ for early transition metal diatomic molecules is made.

1. Introduction

The electric dipole moment, μ, is the most fundamental electrostatic property of a neutral molecule. It is of great utility in the construction of molecular orbital based models of bonding, being an effective gauge of the ionic character, [1, 2]. It enters into the description of numerous physical phenomena. Fermi and Teller established long ago [3] that a neutral closed shell molecule with values of μ greater than 1·625 debye (D) can capture an electron in its electrostatic dipole field, resulting in bound electronic states for the anion. Accordingly, the description of the mobility of electrons through a polar gas relies upon knowledge of μ [4]. It has been realized for decades that the multipole moments, of which μ is the leading term for electrically neutral systems, have proved useful in accounting for intermolecular forces and therefore have helped in the search for an understanding of the macroscopic properties of imperfect gases, liquids and solids. The relationship between the dipole moments of isolated molecules and the macroscopic dielectric constants of dilute gases is given by the famous Debye equation [5]. Similarly, for the liquid phase the Onsager equation [6], and other more recent semi-classical models [7], link the macroscopic static permittivity with μ and the electric polarizability for isolated molecules. Numerous other examples of simple connecting models that allow a prediction of properties of complex systems from the experimentally tractable problem of characterizing the multipoles of isolated molecules can be found in treatises describing intermolecular forces [8, 9].

The permanent electric dipole moment, or its variation with changes in geometry, also enters into the description of light–matter interaction in resonant spectroscopy. Knowledge of the components of the dipole moment along the molecular fixed axis is essential for relative intensity predictions of pure rotational transitions. In this case the Einstein A_{if} and B_{if} rate coefficients for total emission and induced absorption, respectively, are simple functions of the frequency of radiation, an angular momentum dependent line strength factor, and the dipole moment [10–13]. Such information is germane to the transformation of intensities of radiotelescope derived spectra to column densities.

† E-mail: tsteimle@asu.edu

International Reviews in Physical Chemistry ISSN 0144-235X print/ISSN 1366-591X online
http://www.tandf.co.uk/journals

The aforementioned role of the permanent electric dipole moment has been realized for decades. Recently, the availability of experimentally well determined values for μ has become increasingly more important in the assessment of *ab initio* and semi-empirical electronic structure calculations for molecules. The permanent electric dipole moment should be amongst the most reliably predicted physical properties because the quantum mechanical operator describing μ (see below) is a simple sum of one-electron operators. The expectation value of this operator is sensitive primarily to the nature of the least energetic and most chemically relevant valence electrons. Accordingly, a comparison of the experimentally and theoretically derived values of μ is a sensitive test of the general predictive quality of the computational methodology.

A second area of increasing utility of μ is in spatially orientating molecules. The role of μ for electric field orientation of symmetric top molecules in certain rotational levels has been realized for sometime [14, 15]. New impetus for the determination of μ is its importance in experiments introduced independently by Loesch and Remscheid [16] and Friedrich and Herschbach [17] involving spatially orientated non-symmetric top molecules. This 'brute force' approach combines the low rotational temperature achieved in supersonic expansions and the strong interaction of a polar molecule with a homogeneous electric field to restrict the motion of the molecule to a small libration around the axis of the field (i.e., pendular motion). The degree of alignment is dependent upon the magnitude of μ. The approach has been used extensively to study angular distributions in photodissociations [18] and collision processes [19] and in spectroscopy [20, 21].

Here a summary of the current status of experimentally derived values of μ for the 3s, 4s, 5s, and 6s series of metal containing molecules is given. Dipole moment determinations for these transient molecules are particularly challenging because of their refractory nature. In section 2 the experimental methods and resulting data set is accessed. The Stark effect, which is the most commonly used venue for the extraction of μ from spectral data, is summarized in section 3. Particular emphasis is placed upon the complexities unique to metal containing radicals. A detailed comparison of the numerous semi-empirical and *ab initio* predictions is beyond the scope of this review. Comments on the Rittner-type models used for the prediction of the alkaline earth monovalent compounds and the use of simple molecular orbital correlation diagrams to explain observed trends in dipole moments of early and late transition metal mononitrides is given in section 4.

2. Experimental methodologies and determined values

The experimentally determined dipole moments for the 3s, 4s, 5s, and 6s series of metal containing molecules [22–90] are presented in table 1 along with both the statistical (2σ) and systematic error limits when available. In almost all cases the determination of μ was based upon an analysis of how the molecular energy levels of the isolated gaseous species shifted or split as a function of an applied external static electric field: i.e., the Stark effect. As shown in section 3, the Stark effect depends only upon the modulus of μ, therefore only the magnitude of μ has been determined. Unless otherwise indicated, only the lowest vibrational level of a particular electronic state is given. In many cases there is extensive information for excited vibrational levels. Table 1 reveals that the database for diatomic species is much more extensive than for polyatomic molecules. The values of the μ for the more complex molecules in some instances can be approximated as the summation of bond dipole moments extracted

Table 1. Permanent electric dipole moments (in debyes) of 3s, 4s, 5s, and 6s metal containing molecules.

Molecule	Electronic state	$\|\mu\|$ (D)	Error		Exp. method		Ref.
			Stat.	Sys.	Spectrosc.[a]	Production[b]	
NaOH	$X^1\Sigma^+$	6·832	0·009	0·07%	FTMW	LA	[22]
NaF	$X^1\Sigma^+$	8·156	0·001		MBER	Eff.	[23]
NaCl	$X^1\Sigma^+$	9·00090	5×10^{-4}		MBER	Eff.	[24]
NaBr	$X^1\Sigma^+$	9·1183	0·0006		HTMW	Eff.	[25]
NaI	$X^1\Sigma^+$	9·236	0·003		HTMW	Eff.	[25]
MgNC	$X^2\Sigma^+$	3·42	0·09	2%	MBOpt	LA/R	[26]
	$A^2\Pi_{1/2}$	3·11	0·04	2%	MBOpt	LA/R	[26]
KOH	$X^1\Sigma^+$	7·415	0·002		MBER	Eff.	[27]
KF	$X^1\Sigma^+$	8·5926	0·0008		MBER	Eff.	[28]
KCl	$X^1\Sigma^+$	10·269	0·001		MBER	Eff.	[29]
KBr	$X^1\Sigma^+$	10·628	0·001		MBER	Eff.	[30]
KI	$X^1\Sigma^+$	10·82	0·10		MBD	Eff.	[31]
KNa	$D^1\Pi(v=1)$	2·4	0·1		Opt.	Eff.	[32]
CaF	$X^2\Sigma^+$	3·07	0·07	2%	MBDR	Eff.	[33]
	$A^2\Pi$	2·45	0·006	1%	MBOpt	Eff.	[34]
	$B^2\Sigma^+$	2·07	0·15	1%	MBOpt	Eff.	[35]
	$C^2\Pi^+$	9·24	0·17	1%	MBOpt	Eff.	[34]
CaCl	$X^2\Sigma^+$	4·257	0·003	0·1%	MBDR	Eff.	[36]
	$A^2\Pi^+$	3·54	0·10	1%	MBOpt	Eff.	[37]
	$B^2\Sigma^+$	4·03	0·06	1%	MBOpt	Eff.	[37]
CaBr	$X^2\Sigma^+$	4·364	0·003	0·1%	MBDR	Eff.	[38]
CaI	$X^2\Sigma^+$	4·597	0·005	0·1%	MBDR	Eff.	[39]
CaOH	$X^2\Sigma^+$	1·46	0·06	2%	MBOpt	LA/R	[40]
	$A^2\Pi_{1/2}$	0·83	0·03	2%	MBOpt	LA/R	[40]
	$A^2\Pi_{3/2}$	0·76	0·02	2%	MBOpt	LA/R	[40]
	$B^2\Sigma^+$	0·74	0·08	2%	MBOpt	LA/R	[40]
CaNC	$X^2\Sigma^+$	6·89	0·01	2%	MBOpt	LA/R	[41]
	$A^2\Pi_{1/2}$	5·94	0·01	2%	MBOpt	LA/R	[41]
CaSH	X^2A'	5·36	0·04	2%	MBOpt	LA/R	[42]
	B^2A	3·78	0·07	2%	MBOpt	LA/R	[42]
$CaNH_2$	X^2A_1	1·74	0·01	2%	MBOpt	LA/R	[43]
CaCCH	$X^2\Sigma+$	3·01	0·03	2%	MBOpt	LA/R	[44]
	$A^2\Pi_{1/2}$	2·41	0·02	2%	MBOpt	LA/R	[44]
$CaCH_3$	X^2A_1	2·62	0·03	2%	MBOpt	LA/R	[45]
	A^2E	1·69	0·02	2%	MBOpt	LA/R	[45]
$CaOCH_3$	X^2A_1	1·58	0·08	2%	MBOpt	LA/R	[46]
	B^2A_1	1·21	0·05	2%	MBOpt	LA/R	[46]
ScF	$X^1\Sigma^+$	1·72	0·02	2%	MBOpt	LA/R	[47]
	$C^1\Sigma^+$	2·60	0·05	2%	MBOpt	LA/R	[47]
ScO	$X^2\Sigma^+$	4·55	0·08	2%	MBOpt	LA/R	[48]
	$A^2\Pi_{1/2}$	4·42	0·02	2%	MBOpt	LA/R	[48]
	$A^2\Pi_{1/2}$	4·13	0·10	5%	Opt	S	[49]
	$A^2\Pi_{3/2}$	4·06	0·03	2%	MBOpt	LA/R	[48]
	$A^2\Pi_{3/2}$	4·25	0·08	5%	Opt	S	[49]
ScS	$X^2\Sigma^+$	5·60	0·04	2%	MBOpt	LA/R	[50]
	$B^2\Sigma^+$	5·64	0·04	2%	MBOpt	LA/R	[50]
ScNH	$X^2\Sigma^+$	2·28	0·15	2%	MBOpt	LA/R	[51]
	$A^2\Pi$	4·08	0·07	2%	MBOpt	LA/R	[51]
TiH	$X^4\Phi(\Omega=3/2)$	2·455	0·006	2%	MBOpt	LA/R	[52]
	$^4\Gamma(\Omega=5/2)$	2·998	0·006	2%	MBOpt	LA/R	[52]
TiO	$X^3\Delta$	2·96	0·05	3%	IMF	FR	[53]

Table 1. (*cont.*)

Molecule	Electronic state	$\|\mu\|$ (D)	Error		Exp. method		Ref.
			Stat.	Sys.	Spectrosc.[a]	Production[b]	
TiS	$X^3\Delta_1$	5·75	0·10	2%	MBOpt	LA/R	[54]
	$C^3\Delta_1$	4·41	0·09	2%	MBOpt	LA/R	[54]
TiN	$X^2\Sigma^+$	3·56	0·05	2%	MBOpt	LA/R	[55]
	$A^2\Sigma^+$	4·63	0·04	2%	MBOpt	LA/R	[55]
VN	$X^3\Delta_1$	3·07	0·07	2%	MBOpt	LA/R	[56]
	$D^3\Pi_{0e}$	6·1	0·4	2%	MBOpt	LA/R	[56]
VO	$X^4\Sigma^-$	3·355	0·014	0·07%	FTMW	LA	[57]
CrN	$X^4\Sigma^-$	2·31	0·04	2%	MBOpt	LA/R	[56]
	$A^4\Pi_{3/2}$	5·42	0·02	2%	MBOpt	LA/R	[56]
CrO	$X^5\Pi$	3·88	0·13	5%	IMF	FR	[58]
	$B^5\Pi$	4·1	1·8	5%	IMF	FR	[58]
FeO	$X^5\Delta$	4·7	0·2	5%	IMF	FR	[59]
	$\Omega = 2$	2·6	0·2	5%	IMF	FR	[59]
CuF	$X^1\Sigma^+$	5·77	0·20		HTMW	Eff	[60]
CuO	$X^2\Pi_{3/2}$	4·45	0·30	5%	IMF	S	[61]
CuS	$X^2\Pi_{3/1}$	4·32	0·15	5%	IMF	FR	[62]
NiH	$X^2\Delta_{5/2}$	2·4	0·1		Opt.	S	[63]
	$B^2\Delta_{5/2}$	0·3	0·1		Opt.	S	[63]
RbF	$X^1\Sigma^+$	8·5465	0·0005		MBER	Eff.	[64]
RbCl	$X^1\Sigma^+$	10·510	0·005		MBER	Eff.	[64]
RbBr	$X^1\Sigma^+$	10·86	0·10		MBD	Eff.	[31]
RbI	$X^1\Sigma^+$	11·48	0·20		MBD	Eff.	[31]
SrF	$X^2\Sigma^+$	3·4963	0·0006	0·1%	MBDR	Eff.	[65]
	$A^2\Pi$	2·06	0·05	1%	MBOpt	Eff.	[66]
	$B^2\Sigma^+$	0·91	0·04	1%	MBOpt	Eff.	[66]
SrO	$X^1\Sigma^+$	8·900	0·003		MBER	Eff.	[67]
YF	$X^1\Sigma^+$	1·82	0·08	2%	MBOpt	LA/R	[68]
	$B^1\Pi$	2·96	0·04	2%	MBOpt	LA/R	[68]
YCl	$X^1\Sigma^+$	2·587	0·029	2%	MBOpt	LA/R	[69]
	$C^1\Sigma^+$	3·258	0·036	2%	MBOpt	LA/R	[69]
YH	$B^1\Pi$	2·36	0·02	2%	MBOpt	LA/R	[70]
	$C^1\Pi$	3·37	0·02	2%	MBOpt	LA/R	[70]
YO	$X^2\Sigma^+$	4·524	0·007	0·07%	FTMW	LA	[71]
	$A^2\Pi_{1/2}$	3·22	0·02	2%	MBOpt	Eff.	[72]
	$A^2\Pi_{3/2}$	3·68	0·02	2%	MBOpt	Eff.	[72]
YS	$X^2\Sigma^+$	6·098	0·064	2%	MBOpt	LA/R	[73]
	$B^2\Sigma^+$	4·572	0·092	2%	MBOpt	LA/R	[73]
YNH	$X^2\Sigma^+$	3·33	0·07	2%	MBOpt	LA/R	[74]
	$A^2\Pi$	4·52	0·08	2%	MBOpt	LA/R	[74]
	$B^2\Sigma^+$	1·97	0·03	2%	MBOpt	LA/R	[74]
ZrO	$X^1\Sigma^+$	2·551	0·011	0·07%	FTMW	LA	[71]
ZrO_2	X^1A_1	7·80	0·02	0·07%	FTMW	LA	[75]
NbN	$X^4\Delta_1$	3·260	0·016	2%	MBOpt	LA/R	[76]
	$B^4\Phi_2$	4·421	0·010	2%	MBOpt	LA/R	[76]
NbO	$X^4\Sigma^-$	3·498	0·007	0·07%	FTMW	LA	[57]
MoN	$X^4\Sigma^-$	2·44	0·05	2%	MBOpt	LA/R	[77]
	$A^4\Pi$	4·55	0·04	2%	MBOpt	LA/R	[77]
AgF	$X^1\Sigma^+$	6·22	0·20		HTMW	Eff.	[60]
AgCl	$X^1\Sigma^+$	5·70	0·015		HTMW	Eff.	[78]
CsF	$X^1\Sigma^+$	7·8839	0·0009		HTMW	Eff.	[25]
CsCl	$X^1\Sigma^+$	10·387	0·004		HTMW	Eff.	[25]
CsBr	$X^1\Sigma^+$	10·82	0·10		MBD	Eff.	[31]

Table 1. (*cont.*)

Molecule	Electronic state	$\|\mu\|$ (D)	Error		Exp. method		Ref.
			Stat.	Sys.	Spectrosc.[a]	Production[b]	
CsI	$X\,^1\Sigma^+$	11·69	0·10		MBD	Eff.	[31]
BaF	$X\,^2\Sigma^+$	3·170	0·003	0·1%	MBDR	Eff.	[79]
	$B\,^2\Sigma^+$	0·38	0·09	1%	MBopt	Eff.	[35]
BaI	$X\,^2\Sigma^+$	5·969	0·006	1%	MBDR	Eff.	[80]
BaO	$X\,^1\Sigma^+$	7·955	0·003		MBER	Eff.	[81]
	$A\,^1\Sigma^+$	2·20	0·11		MODR	FR	[82]
BaS	$X\,^1\Sigma^+$	10·86	0·02		MBER	Eff.	[83]
LaF	$X\,^1\Sigma^+$	1·808	0·021	2%	MBOpt	LA/R	[84]
	O^+	3·43	0·10	2%	MBOpt	LA/R	[84]
LaO	$X\,^2\Sigma^+$	3·207	0·011	0·07%	FTMW	LA	[71]
HfO_2	$X\,^1A_1$	7·92	0·02	0·07%	FTMW	LA	[85]
IrC	$X\,^2\Delta_{5/2}$	1·60	0·07	2%	MBOpt	LA/R	[86]
	$D\,^2\Phi_{5/2}$	2·61	0·06	2%	MBOpt	LA/R	[86]
IrN	$X\,^1\Sigma^+$	1·66	0·01	2%	MBOpt	LA/R	[86]
	$A\,^1\Pi$	2·78	0·02	2%	MBOpt	LA/R	[86]
PtC	$X\,^1\Sigma^+$	1·08	0·04	2%	MBOpt	LA/R	[87]
	$A''\,^1\Sigma^+$	1·94	0·02	2%	MBOpt	LA/R	[88]
	$A'\,^1\Pi$	1·919	0·009	2%	MBOpt	LA/R	[88]
	$A\,^1\Pi$	2·455	0·002	2%	MBOpt	LA/R	[88]
PtN	$X\,^2\Pi_{1/2}$	1·977	0·009	2%	MBOpt	LA/R	[89]
	$d\,^4\Pi_{1/2}$	1·05	0·011	2%	MBOpt	LA/R	[89]
PtO	$X(\Omega = 0)$	2·77	0·02	2%	MBOpt	LA/R	[90]
	$B(\Omega = 0)$	1·15	0·04	2%	MBOpt	LA/R	[90]
PtS	$X(\Omega = 0)$	1·78	0·02	2%	MBOpt	LA/R	[90]
	$B(\Omega = 0)$	0·54	0·06	2%	MBOpt	LA/R	[90]
PtSi	$X\,^1\Sigma^+$	1·08	0·04	2%	FTMW	LA/R	[85]

[a] Spectroscopic technique: HTMW, high temperature microwave/Stark; FTMW, Fourier transform microwave/Stark; MBOpt, molecular beam optical/Stark; Opt, Doppler limited optical/Stark; IMF, intermodulated fluorescence/Stark; MODR, microwave/optical double resonance; MBER, molecular beam electric resonance; MBD, molecular beam deflection.
[b] Molecular production scheme: LA/R, laser ablation/reaction; Eff, effusive oven; FR, flowing reactor; S, sputtering.

from the measurements for the diatomic compounds. This is particularly true for van der Waals complexes.

Early studies of electric dipole moments of refractory molecules employed molecular beam electric resonance (MBER) [23, 24, 27–30, 64, 67, 81, 83] and molecular beam deflection (MBD) [31] techniques or high temperature microwave (HTMW) [25, 60, 78] spectroscopy. A review of MBER and MBD can be found in the classical book by Ramsey [91]. A review of the HTMW approach can be found in standard books on microwave spectroscopy [11, 12] and in the article by Lovas and Hide [92]. The MBER measurements involved recording either microwave frequencies for transitions between electric field split levels associated with two different rotational states or radiofrequencies for transitions between electric field split levels within a given rotational state. Generally the high temperature microwave measurements involved transitions between electric field split levels associated with two different rotational states. The almost exclusive use of effusive oven sources in these early studies restricted molecular production primarily to the alkali and alkaline earth

monohalides and monoxides. A review of electric dipole moments of refractory molecules measured by MBER and HTMW, circa 1970, can be found in [92] and [93].

In the 1980s Ernst and Törring in Berlin [38, 39, 65, 79, 80] and Childs and Goodman [33] at Argonne National Laboratory developed molecular beam double-resonance (MBDR) techniques with the ability to perform Stark measurements. Precise measurements of electric dipole moments for numerous alkaline earth monohalides in their ground electronic state were performed. The MBDR technique is the optical analogue of the MBER method, with the molecules being exposed sequentially to three radiation fields. The state selection (A field) and detection (B field) electric fields of the conventional MBER experiment were replaced by optical pumping and optical detection via laser induced fluorescence (LIF). The C field region where the microwave or RF resonance is driven in the presence of a uniform electric field was essentially identical to that of the MBER spectrometer. A review of those studies can be found in [94].

Ernst and Törring also performed high resolution molecular beam optical (MBOpt) Stark measurements on a number of the same alkaline earth monohalides to determine μ for their excited electronic states [34, 35, 66]. The molecular beam conditions, coupled with the use of single-frequency laser excitation, provided the necessary spectral resolution (typically less than 50 MHz full width at half maximum (FWHM)) to detect the relatively small induced Stark shifts and splittings of the optical spectral features for these molecules. High temperature effusive ovens served as the molecular source, restricting the types of molecule that could be probed. About the same time, Field's group at MIT performed optical (Opt) Stark studies on 'bulb' samples of ScO [49] and NiH [63]. These radical molecules were produced by a more versatile flowing reactor scheme in which the metal vapour was generated in a hollow cathode sputtering source. The rapid electric tuning rate of the selected energy levels for these molecules produced Stark shifts greater than the Doppler broadened line widths of approximately 1 GHz for the optical transition. Encouraged by their success, we initiated a series of optical Stark studies on 'bulb' samples [53, 58, 59, 61, 62] at Arizona State University (ASU), but using the saturation technique of intermodulated fluorescence (IMF) spectroscopy [95] to reduce the linewidth of the optical spectral features to less than 100 MHz. Although a wider range of molecules could be produced using the flowing reactor scheme, only moderately high electric fields (< 100 V cm^{-1}) could be achieved because of the operating pressure.

The introduction of the laser ablation/reaction source developed about a decade ago [96–99] significantly expanded the range of metal containing gas phase molecules that could be studied. In this approach a short intense pulse of radiation, usually originating from a Nd:YAG laser, is focused on a metal or metal containing sample target. The plume of vaporized product is entrained in a supersonic expansion of an inert/reagent gas mixture. Lovas and Suenram at NIST have coupled the laser ablation/reaction source to a Fourier transform microwave (FTMW) spectrometer for the precise determination of ground state electric dipole moments of transition metal monoxides [57, 71], dioxides [75, 85], NaOH [22] and PtSi [85]. About the same time Simard's group at NRC-Ottawa began to use the source in high resolution MBOpt Stark studies, and have determined electric dipole moments for both the ground and excited electronic states of ScF [47], TiH [52], TiN [55], YF [68], YH [70], YS [73], YNH [74] and LaF [84]. Soon thereafter we began similar experiments at ASU and have performed MBOpt Stark measurements on a series of alkaline earth monovalent molecules [26, 40–46], transition metal monoxides [48, 72, 90], mono-

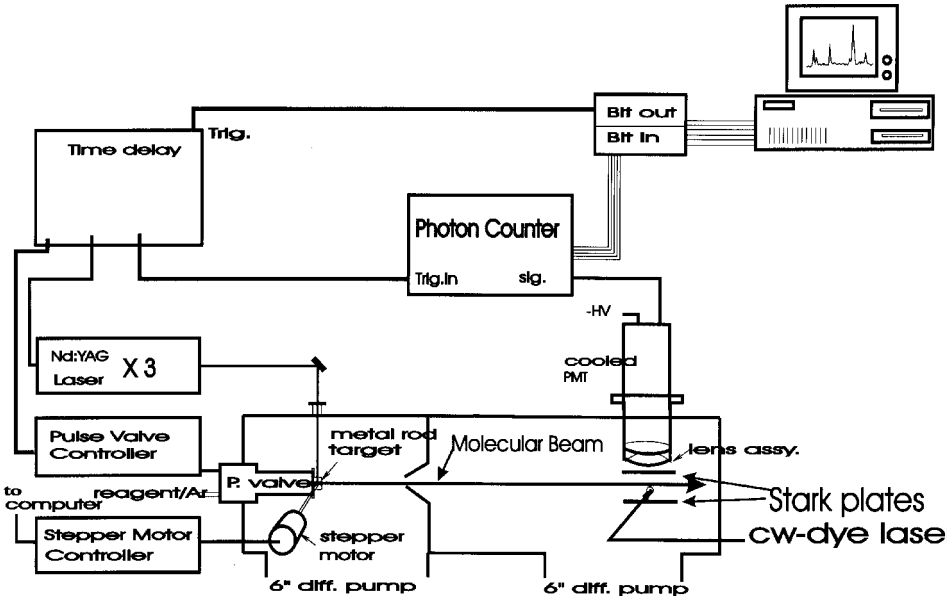

Figure 1. Block diagram of the molecular beam optical Stark spectrometer. The separation between the laser ablation source and the LIF detection region is approximately 60 cm, facilitating easy discrimination of background light from the plasma.

sulphides [50, 54, 90], monohydrides [52], mononitrides [56, 76, 77, 86, 89], monocarbides [86–88], and ScNH [51].

The schematic of the molecular beam optical Stark spectrometer used at ASU is presented in figure 1. The free jet expansion is skimmed to produce a well collimated molecular beam. This has the effect of reducing the linewidth to approximately 40 MHz (FWHM) and increasing the limit of applied electric field to approximately 10 kV cm^{-1} because of the lower operating pressure to (5×10^{-6} Torr). The Stark plates consist of one solid polished stainless plate and a metallic coated 99% transmissive neutral density filter. The LIF signal is collected through a narrow ($\pm$10 nm) bandpass filter and processed using gated photon counting signal averaging. The pulse molecular beam operates at a 20 Hz repetition. The 60 cm separation between the ablation source and the detection region allows for easy discrimination of the LIF signal from the plasma emission. The absolute wavelength of the laser light is determined to $\pm$90 MHz by the comparison with a standard absorption spectrum of I_2. The relative wavelength is determined to typically $\pm$2 MHz by monitoring the transmission of a temperature stabilized and calibrated 1 m confocal étalon.

As expected, the most precise values for μ are derived from an analysis of Stark effects on pure rotational transitions recorded by MBER, HTMW, MBDR or FTMW techniques. The exceedingly high resolution obtainable (< 10 kHz FWHM), means that precise electric field dependence of the energy levels can be achieved. The absolute transition frequencies are measured accurately using electronic counting. Typically the accuracy of these measurements is limited by systematic errors associated with the calibration of the static field. The precision of a MBOpt Stark measurement is significantly less because of limitations in measuring the relative optical transition frequencies. The optical Stark spectra are sensitive primarily to the difference in the ground and excited electronic state dipole moments. Correlation between the two

values can be significant unless a number of optical transitions over a range of applied static electric fields are measured. The optical and IMF measurements are the least accurate because of poor spectral resolution and parameter correlation effects.

3. The Stark effect

3.1. *General*

All of the electric dipole moments of table 1 resulted from the interpretation of the effect of an applied electric field on the absorption or emission spectra; i.e., the Stark effect. This technique permits the measurement of the dipole moments in particular stationary states, as distinct from the average moments extracted from dielectric constants using the Debye equation [5]. Even if it were possible to measure the dielectric constant for a room temperature gas sample of these transient molecules, the value of the dipole moment extracted from the Debye equation would be significantly different from those given in table 1 because of the high density of populated interacting low lying states. The importance of the Stark spectroscopy of gaseous samples for the determination of μ has long been realized, and a thorough development of the theory can be found in classical texts of molecular spectroscopy [10–13] and in the review articles by Buckingham [93, 100]. An overview of the approach is still warranted because the nonzero nuclear and electronic spin and high density of levels characteristic of the metal containing molecules makes the interpretation more complex than that typically described in the standard texts.

The classical energy W of a neutral molecule exposed to a homogeneous electric field $\mathbf{E}$ can be expressed as a power series of that field, and to the first two terms is

$$W = W^0 - \boldsymbol{\mu}\cdot\mathbf{E} - \tfrac{1}{2}\mathbf{E}\cdot\boldsymbol{\alpha}\cdot\mathbf{E} + \ldots. \tag{1}$$

Here W^0 is the field free energy, $\boldsymbol{\mu}$ is the electric dipole moment vector with the components being defined as

$$\mu_\alpha \equiv \sum_\alpha \left(\frac{\partial W}{\partial E_\alpha}\right)_{E_\alpha = 0} \tag{2}$$

and $\boldsymbol{\alpha}$ is polarizability tensor whose components are defined as

$$\alpha_{\alpha\beta} \equiv \sum_{\alpha,\beta} \left(\frac{\partial^2 W}{\partial E_\alpha \partial E_\beta}\right)_{E_{\alpha,\beta} = 0.} \tag{3}$$

In equations (2) and (3) the summation runs over the three components of the laboratory fixed Cartesian coordinate axes system. The classical energy contribution due to the electric polarization can be written as $\frac{1}{2}\mathbf{E}\cdot\boldsymbol{\mu}^{\mathrm{ind}}$ with $\boldsymbol{\mu}^{\mathrm{ind}} \equiv \Sigma_\beta \alpha_{\alpha\beta} E_\beta$ being the electric field induced dipole moment. Viewing the molecule as a collection of discrete particles of charge e_{i} located in space by the position vector $\mathbf{r}_i$ then equation (2) becomes [93]

$$\boldsymbol{\mu} = \sum_{i=1}^{N} e_i \mathbf{r}. \tag{4}$$

The last two terms of equation (1) are sufficient to account for all known molecular interactions with a homogeneous, static, electric field. Therefore an appropriate

quantum mechanical operator written in terms of the molecule fixed components of the electric dipole moment operator $\hat{\mu}^{\text{mol}}$ and electric polarizability operator $\hat{\alpha}^{\text{mol}}$ is

$$\hat{H}^{\text{Stark}} - \hat{\mu}^{\text{mol}} \cdot \tilde{\mathbf{C}} \cdot \mathbf{E} - \tfrac{1}{2}\mathbf{E} \cdot \mathbf{C}\hat{\alpha}^{\text{mol}} \cdot \tilde{\mathbf{C}} \cdot \mathbf{E} + \ldots \quad (5)$$

In equation (5) the direction cosine matrices $\mathbf{C}$, and inverse $\tilde{\mathbf{C}}$, perform the necessary laboratory-to-molecule and molecule-to-laboratory transformation of the co-ordinates, respectively. Assuming that the total stationary state wavefunctions can be written as the product of an electronic, vibration, rotation, electronic spin and nuclear spin function that has definite parity p, then the 'permanent' electric dipole moment is defined as

$$\mu \equiv \left\langle \Psi^{\text{el.}} \Psi^{\text{vib.}} \Psi^{\text{rot.}} \Psi^{\text{el.sp.}} \Psi^{\text{nuc.sp.}}; p | \hat{\mu} | \Psi^{\text{el.}} \Psi^{\text{vib.}} \Psi^{\text{rot.}} \Psi^{\text{el.sp.}} \Psi^{\text{nuc.sp.}}, p \right\rangle. \quad (6)$$

A molecule in a non-degenerate state has no 'permanent' electric dipole moment *per se* as defined by equation (6) because $\hat{\mu}^{\text{mol}}$ is of odd parity and its expectation value must vanish. The average electric dipole moment in the laboratory frame is zero because of the random orientation of the molecules in space. Molecules having degenerate electronic states of opposite parity can possess a 'permanent' electric dipole moment because even in an infinitesimally small applied electric field the parity of the electronic states will be destroyed. A more appropriate quantum mechanical definition of the permanent electric dipole is an expectation over the electronic wavefunction.

The procedure for determining the Stark effect of a given quantum level is a matter of selecting a basis set, generating the representation of the total Hamiltonian operator inclusive of $\hat{H}^{\text{Stark}}$, and performing a numerical diagonalization to extract the energies. Implicit in this procedure is the assumption that the spectral information is extensive enough to fully characterize the field free energies. It is convenient to recast $\hat{H}^{\text{Stark}}$ into spherical tensor form and to use spherical tensor algebra to evaluate the matrix elements of $\hat{H}^{\text{Stark}}$ and $\hat{H}^{0}$, the field free Hamiltonian operator. In spherical tensor form equation (5) becomes [11, 101, 102]

$$\hat{H}^{\text{Stark}} = -\sum_{q,\,p} (-1)^{p} T^{1}_{p}(E)\, D^{*}_{-pq}(\omega) T^{1}_{q}(\mu) - \sum_{k=0}^{2} \sum_{q,\,p} (-1)^{p} T^{k}_{p}(EE)\, D^{*}_{-pq}(\omega) T^{k}_{q}(\alpha). \quad (7)$$

In equation (7) $D^{*}_{pq}(\omega)$ is the complex conjugate of the Wigner rotation matrix, with ω representing the Euler angles. The notation $T^{k}_{p}(EE)$ represents the kth rank spherical tensor operator formed from the decomposition of the second-rank Cartesian tensor formed from the tensor product $T^{1}_{p}(E) \otimes T^{1}_{p}(E)$. The molecule-fixed axes are designated with q and the space fixed axes with p.

It is necessary to justify the omission of the polarization contribution to the Stark shift. This can be achieved by considering a closed shell linear molecule in a non-degenerate state. The Stark shift given by second-order perturbation theory in this case is [10]

$$E^{\text{Stark}}(J, M_J) = -E_z^2 \left[\frac{3M_J - J(J+1)}{(2J-1)(2J+3)} \right] \times \left[\frac{\mu^2}{2hBJ(J+1)} - \frac{1}{3}(\alpha_{aa} - \alpha_{bb}) \right] - \frac{1}{2} E_z^2 \alpha, \quad (8)$$

where α is the average polarizability ($\equiv(\alpha_{aa}+\alpha_{bb}+\alpha_{cc})/3$). Assuming an anisotropic polarizability $(\alpha_{aa} - \alpha_{bb}) = \alpha \approx 20 \times 10^{-24}$ cm^{-1} [103], a rotational constant B of 5 GHz, a dipole moment of 1 D and an applied field 5000 V cm^{-1} then the $M_J = 1$, $J = 1$ level has contributions of -0.34 kHz and 103 MHz, from the anisotropic polarizability and dipole terms, respectively. The isotropic term contributes only a constant to the

energy and will not effect the transition frequency. None of the measurements in table 1, with the possible exception of the most sensitive MBER or FTMW results, has the precision to determine the polarization effect and this will be ignored from here on.

3.2. *Linear molecules*

The linear metal containing molecules of table 1 typically have spin–spin and spin–orbit interactions that are much larger than the spacing between the lowest rotational energies. In this case the electronic spin angular momenta are quantized in the molecule fixed axis system and case $a_{\beta,J}$ basis set formed by taking the product of the electronic orbital, $|n\Lambda\rangle$, electronic spin $|S\Sigma\rangle$ and a coupled function of the rotational and nuclear spin angular momenta, $|(JI)F\Omega M_F\rangle$, is appropriate:

$$|\Psi(\text{case } a_{\beta J}\rangle = |n\Lambda\rangle\,|S\Sigma\rangle\,|JIF\Omega M_F\rangle.$$

The matrix elements of $\hat{H}^{\text{Stark}}$ in a case $a_{\beta J}$ basis set are then evaluated as

$$\begin{aligned}\langle n\Lambda;S\Sigma;JI\Omega M_F|\hat{H}^{\text{Stark}}|n\Lambda';S\Sigma';J'I\Omega' m'_F\rangle = \\ -E\langle n\Lambda|T^1_0(\mu)|n\Lambda'\rangle\,(-1)^{F-M_F}\begin{pmatrix} F & 1 & F' \\ M_F & 0 & M_F \end{pmatrix} \\ \times(-1)^{J+I+F'+1}[(2F+1)(2F'+1)]^{1/2}\begin{Bmatrix} I & J & F \\ I & F' & J' \end{Bmatrix} \\ \times(-1)^{J-\Omega}[(2J+1)(2J'+1)]^{1/2}\begin{pmatrix} J & 1 & J' \\ -\Omega & 0 & \Omega \end{pmatrix}. \quad (9)\end{aligned}$$

The representation is block diagonal in M_F but of infinite dimension. As indicated in figure 2, each of the diagonal blocks is specified by the total angular momentum F and is in general of $2(2S+1)(2I_1+1)(2I_2+1)\ldots$ dimension. If the Λ doubling and hyperfine splittings are negligible and the induced Stark shift is significantly less than the spacing between the adjacent rotational levels then the Stark shift can be approximated as:

$$E^{\text{Stark}}(J, M_J) = (0{\cdot}5034\ \text{MHz D}^{-1}\ V^{-1}\ \text{cm})\times\left[\frac{\mu|M_J|\Omega}{J(J+1)}\right]. \quad (10)$$

As an example of a Stark interaction in a linear molecule with hyperfine interaction consider IrN [86]. The (1,0) $R(0)$ (v = 16070·4 cm^{-1}) branch feature of the A $^1\Pi-$X $^1\Sigma^+$ band system for the ^{193}IrN isotopomer recorded under field free conditions and in the presence of a 179 V cm^{-1} and a 1013 V cm^{-1} electric field is presented in figure 3. The splitting is due to the magnetic hyperfine ($\hat{H}^{\text{mhf}} = a\hat{I}\cdot\hat{L}$) interaction between the electronic orbital angular momentum and the nonzero nuclear spin of ^{193}Ir(I = 3/2). The ^{14}N(I = 1) hyperfine interactions are not resolved in the optical spectra. In these spectra the static electric field was oriented perpendicular ($\perp$) to the electric field vector of the nominally linearly polarized laser light, resulting in $\Delta M_F = \pm 1$ optical selection rules. The three field-free spectral features at 16069·835 cm^{-1}, 16069.847 cm^{-1}, and 16069·865 cm^{-1} are assigned as the J'' = 0, F'' = 3/2 to J' = 1, F' = 5/2, 3/2 and 1/2 transitions, respectively. At low electric field strengths these three transitions split rapidly into $2F'+1$ components as expected for the A $^1\Pi$ state, which has negligible Λ doubling. The X $^1\Sigma^+$ state exhibits only a small second-order Stark shift. At high electric field strength the spectrum appears as three groups (= $2J'+1$) of four (= $2I+1$) nearly equally spaced features. In this strong field

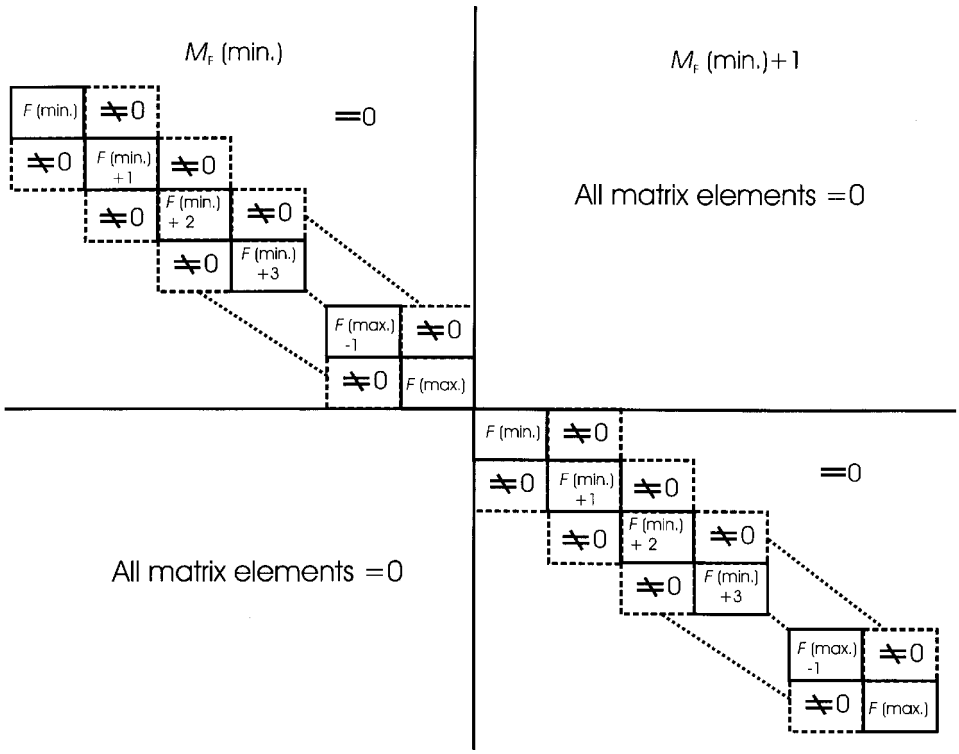

Figure 2. Appearance of the matrix representation of $\hat{H}^{\text{Stark}}$. In a case $a_{\beta J}$ appropriate for a linear molecule with large spin–spin and spin–orbit interactions each of the diagonal blocks is $2(2S+1)(2I_1+1)(2I_2+1)\ldots$ in dimension. In a case $b_{\beta J}$ basis appropriate for a nonlinear molecule the diagonal blocks is $(2S+1)(2I_1+1)(2I_2+1)(2F+1)\ldots$ in dimension. The matrix is truncated at a maximum F selected to be commensurate with the accuracy of the experimental measurement.

the nuclear spin becomes decoupled from the rotational angular momentum, and the approximately good quantum numbers are M_I and M_J. This corresponds, classically, to the rotational angular momentum and the nuclear spin angular momentum individually precessing about the field, and is analogous to the familiar Paschen–Back effect observed in strong magnetic fields. The final optimized spectroscopic parameters and determined dipole moments were used to generate the energy level diagram plotted as a function of applied electric field in figure 4.

Analysis of the Stark effect for the (1,0) $R(0)$ (ν = 16070·4 cm^{-1}) branch feature A $^1\Pi$–X $^1\Sigma^+$ band system of IrN required constructing a 26×26 matrix representation to model the Stark effect for the J = 1 level of the A $^1\Pi$ state and a 10×10 matrix representation to model the Stark effect for the J = 0 level of the X $^1\Sigma^+$ state. The matrix representations were truncated at these finite sizes because it was determined to be commensurate with the experimental accuracy (~ 20 MHz). The matrix for the A $^1\Pi$ state was composed of 4×4, 6×6, 8×8, and 8×8 blocks for the F = 0·5, 1·5, 2·5 and 3·5 field free representations along with connecting matrix elements due to $\hat{H}^{\text{Stark}}$. This accounted for both the first-order Stark effect between the degenerate Λ doublet and second-order contributions between the J' = 1 and J' = 2 sets of hyperfine levels. The 10×10 matrix representation required to model the Stark shift of the J = 0 rotational level in the X $^1\Sigma^+$ was composed of the 2×2, 4×4 and 4×4 field free blocks

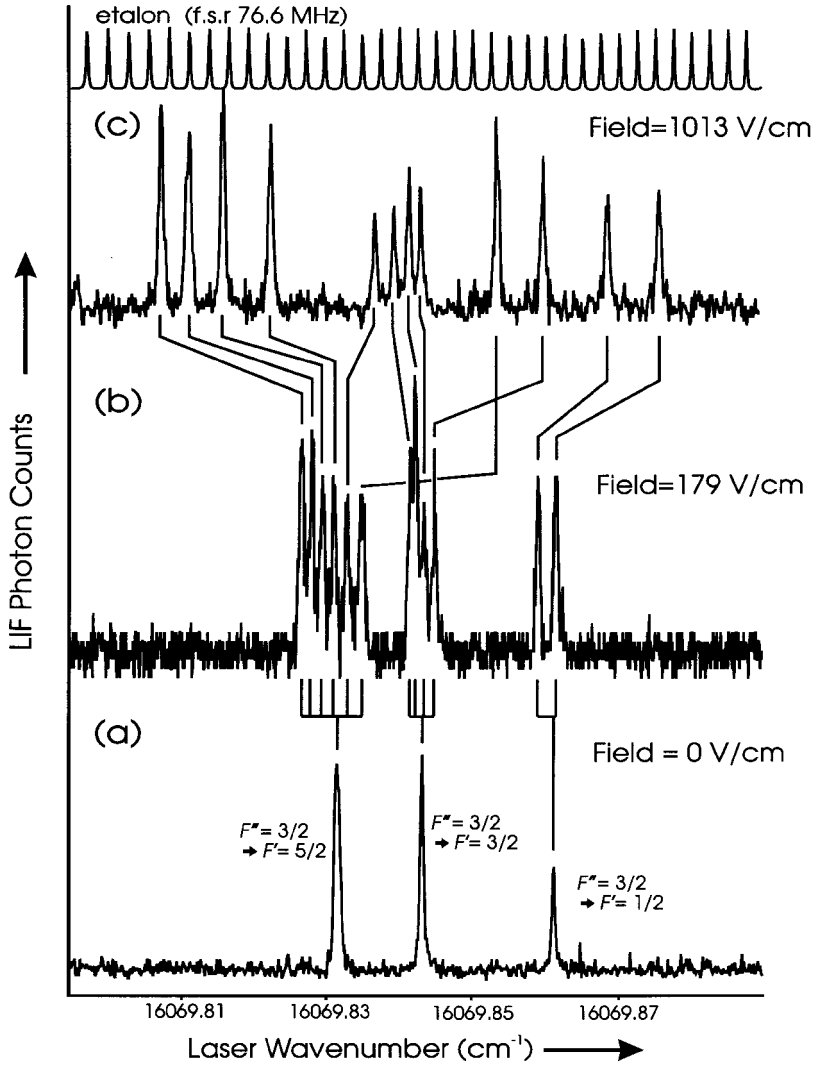

Figure 3. (1,0) $R(0)$ (ν = 16070·4 cm^{-1}) branch feature of the A $^1\Pi$–X $^1\Sigma^+$ electronic transition of IrN recorded: (a) under field free conditions; (b) in the presence of a 179 V cm^{-1} electric field; and (c) in the presence of a 1013 V cm^{-1} electric field. The static electric field was oriented perpendicular ($\perp$) to the electric field vector of the nominally linearly polarized laser light.

for F'' = 1/2, 3/2 and 5/2 levels and the connecting matrix elements due to $\hat{H}^{\text{Stark}}$. This accounted for the entire interaction between the J'' = 0 and J'' = 1 sets of hyperfine levels and the major contribution to the Stark shift of J'' = 0 from the interaction with the J'' = 2 hyperfine levels.

3.3. *Symmetric and asymmetric tops*

The model for the Stark effects in closed shell asymmetric rotors was developed 50 years ago by Golden and Wilson [104]. In this classic work approximate expressions for the energies were derived using second-order perturbation theory. The small rotational constants for most polyatomic metal containing molecules precludes the use

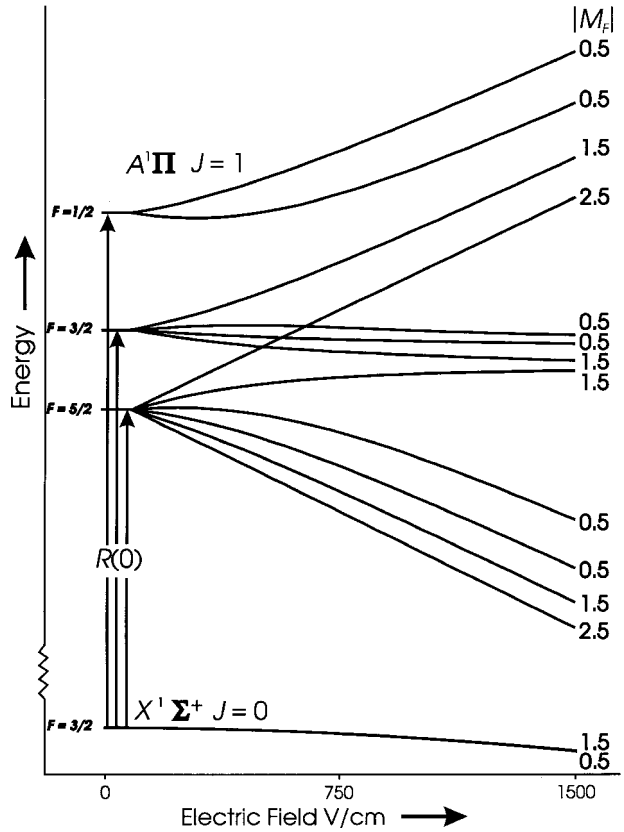

Figure 4. Energy level diagram plotted as a function of applied electric field for the (1,0) $R(0)$ branch feature of the $A^1\Pi$–$X^1\Sigma^+$ electronic transition of IrN. The nuclear spin rapidly decouples from the molecular framework with the application of the electric field.

of these expressions at all but the lowest applied electric field strengths, and an approach analogous to that used for the linear molecules is necessary. The most appropriate basis set for nonlinear open shell polyatomic metal containing molecules has the electronic spin coupled to the rotational motion and the nuclear spins sequentially coupled to the resultant intermediate angular momenta, i.e., a case $b_{\beta J}$ basis [11, 105, 106]:

$$|\Psi(\text{case } b_{\beta J}\rangle = |NKSJIFM_F\rangle. \tag{11}$$

The case $b_{\beta J}$ matrix elements $\hat{H}^{\text{Stark}}$ for a homogeneous applied field are given by [106]

$$\langle NKSJIFM_F|\hat{H}^{\text{Stark}}|N'K'SJ'IF'M'_F = -E_Z(-1)^{F-M_F}\begin{pmatrix} F & 1 & F' \\ M_F & 0 & M_F \end{pmatrix}$$

$$\times(-1)^{J+I+F'+1}[(2F+1)(2F'+1)]^{1/2}\begin{Bmatrix} I & J' & F' \\ 1 & F & J \end{Bmatrix}(-1)^{N+S+J'+1}[(2J+1)(2J'+1)]^{1/2}$$

$$\times\begin{Bmatrix} N & J & S \\ J' & N' & 1 \end{Bmatrix}\sum_q(-1)^{N-K}[(2N+1)(2N'+1)]^{1/2}\begin{pmatrix} N & 1 & N' \\ -K & q & K' \end{pmatrix}\langle|T_q^1(\mu)|\rangle. \tag{12}$$

Again, the representation is diagonal in projection of total angular momentum quantum number M_F, and of infinite size. The dimensions of the field free blocks are $(2S+1)(2I_1+1)(2I_2+1)\ldots(2F+1)$. Unlike for linear molecules, the field free blocks

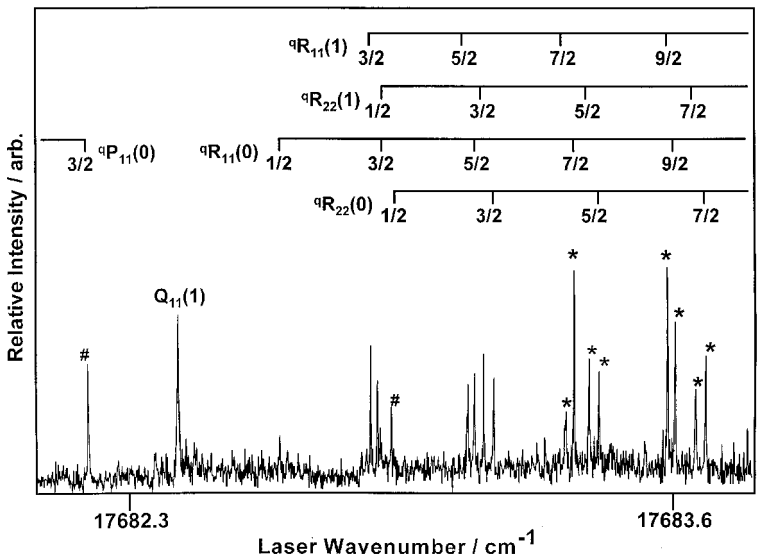

Figure 5. Portion of the field free laser induced fluorescence spectrum near the origin of the (0,0) $B\,^2A_1$–$X\,^2A_1$ band system of $CaOCH_3$. The features marked with a # were used in the optical Stark measurements.

of figure 2 rapidly increase in size with increasing rotational angular momenta. Therefore, it is extremely advantageous to select the lowest rotational levels for Stark investigations. In the absence of nuclear hyperfine and spin–rotation interactions, negligible asymmetry splitting and electric field induced shifts significantly less than the spacing between the rotational levels, then the Stark effect for levels for $K \neq 0$ is given by equation (10) but with J, Ω, and M_J replaced by N, K and M_N.

Consider calcium methoxy, $CaOCH_3$, as an example of a Stark effect for an open shell polyatomic molecule [46]. The alkaline earth monovalent compounds are unique amongst radicals containing a metal bound to a complex ligand in that molecular beam samples can be generated readily and the associated high resolution optical spectra recorded and interpreted readily. This makes them ideal systems for studying ligand dependent trends in bonding. A portion of the field free laser induced fluorescence spectrum near the origin of the $(0,0)\,B\,^2A_1 - X\,^2A_1$ band system of $CaOCH_3$ is given in figure 5. The proton magnetic hyperfine interaction is not resolved at the optical resolution of approximately 40 MHz. The $^qP_{11}(0, 1{\cdot}5)$ (ν = 17 682·1966 cm^{-1}) branch features of the (0, 0) $B\,^2A_1$–$X\,^2A_1$ band system recorded field free and in the presence of a static electric field of 4593 V cm^{-1} is presented in figure 6. (The branch feature designation that has been employed is $^{\Delta|K|}\Delta J_{F_i'F_i''}(|K|'', J'')$.) The spectrum was recorded by turning off/on the electric field midway through the scan in order to measure accurately the induced shift. A $\perp$ orientation of the linearly polarized laser radiation relative to the static electric field was used. The associated energy levels are given in figure 7. The spin–rotation splitting is negligible for the low rotational levels in the $X\,^2A_1$ state, making N and M_N the approximately good quantum numbers, whereas it is substantial in the $B\,^2A_1$ state, making J and M_J the approximately good quantum numbers. This is a typical situation for polyatomic open shell molecules because the spin–rotation interactions are dominated by second-order contributions resulting from the break down of the Born–Oppenheimer approximation.

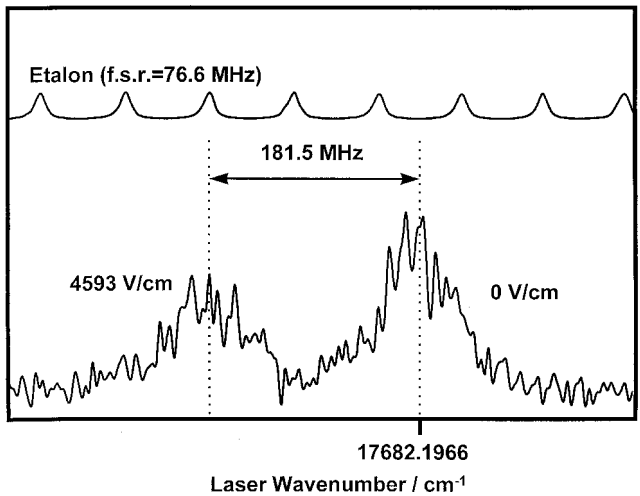

Figure 6. Optical Stark spectrum of the $^{q}P_{11}(0, 1{\cdot}5)$ (ν = 17 682·1966 cm^{-1}) branch features of the (0,0) $B\,^2A_1$–$X\,^2A_1$ band system of $CaOCH_3$. The spectrum was recorded by turning off/on the electric field midway through the scan. The associated energy levels are given in figure 7. A $\perp$ orientation of the linearly polarized laser radiation relative to the static electric field was used.

The Stark shifts in the $B\,^2A_1$ and $X\,^2A_1$ states were modelled by constructing matrix representations in a case *b* basis sets, $\Psi = |N, K, S, J, M_J\rangle$, using equation (12) with the nuclear spin set equal to zero for the evaluation of the matrix elements. The representation was truncated at J = 3·5 resulting in a 40 × 40 dimension matrix. The field free energy levels have to be known accurately prior to an analysis of the second-order Stark shifts as exhibited in this transition. In many instances the optical transitions selection rules preclude a complete determination of the set of field free parameters. In this case the A rotational parameters for the $X\,^2A_1$ and $B\,^2A_1$ states, which dictate the separation between the K = 0 levels and the other rotational stacks of levels of $|K| \neq 0$, were not extractable from the analysis of the optical spectrum, and reasonable estimates had to be assumed.

The optimum estimates of the permanent electric dipole moments $|\mu(X\,^2A_1)|$ = 1·58(8) D and $|\mu(B\,^2A_1)|$ = 1·21 (5) D were obtained using a standard unweighted nonlinear least-squares data reduction procedure. There are no *ab initio* predictions for μ, and a simple electrostatic model (see below) was used to interpret the results. The determined values of $|\mu(X\,^2A_1)|$ and $|\mu(B\,^2A_1)|$ are significantly less than that expected for $Ca^{+1}(OCH_3)^{-1}$ point charge distribution ($\sim$ 9·8 D) due to the induced dipole moments of Ca^+, μ^+, and CH_3O^-, μ^-, and the intrinsic dipole moment of the anion, $\mu(CH_3O^-)$:

$$\mu = er_{CaO} - \mu^+ - \mu^- - \mu(CH_3O^-). \tag{13}$$

Indeed, because the experiments determine only the magnitude of μ, it is possible that the direction of the dipole is opposite to that of a $Ca^{+1}(OCH_3)^{-1}$ point charge distribution. Like $CaCH_3$, where $|\mu(X\,^2A_1)|$ = 2·62(3) D and $|\mu(A\,^2E)|$ = 1·69(2) D [45], the ground state value $|\mu|$ is greater than that of the excited state. The singly occupied a_1 Ca^+ centred orbital of the excited state, which is primarily a 3d–4p ligand induced hybrid orbital, is more polarizable than the singly occupied a_1 Ca^+ centred orbital of the ground state, which is primarily a 3d–4s–4p ligand induced hybrid orbital. This would suggest that the direction of μ is from Ca to O.

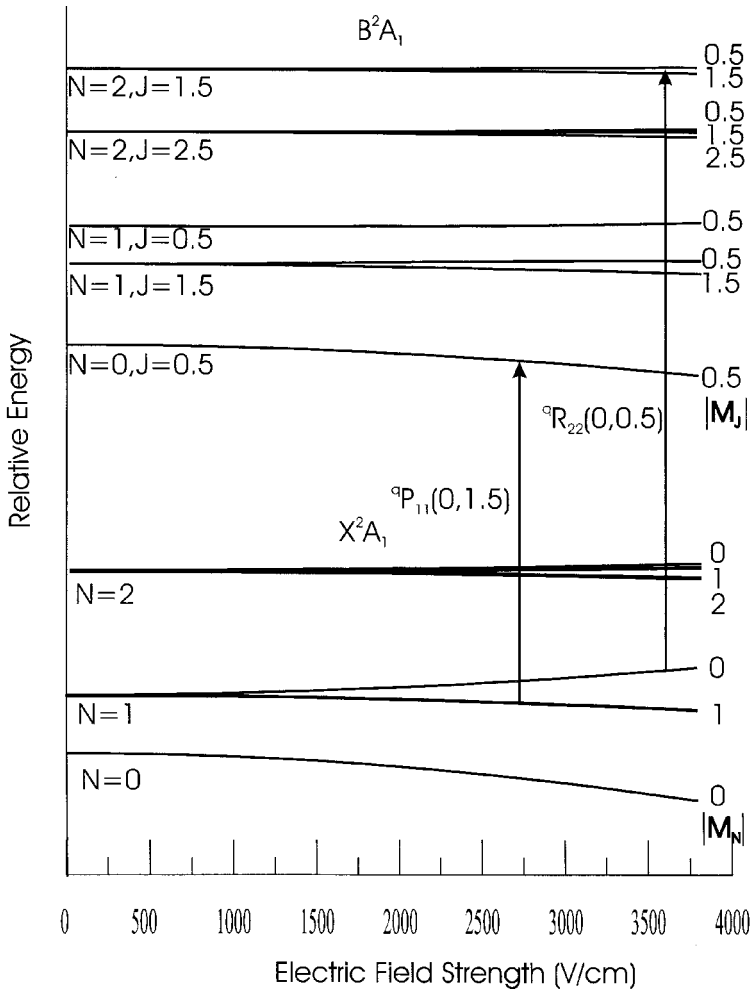

Figure 7. Energy levels as a function of applied electric field. The experimentally determined μ of 1·58 D and 1·21 D for the X^2A_1 and B^2A_1 states, respectively, were used. The rotational splitting is not drawn to scale.

4. Trends in electric dipole moments

The trends in dipole moments of the alkali and alkaline earth monohalides have been investigated thoroughly [94, 40, 43–46, 107, 108] using semi-empirical ionic models based upon Rittner's original work [109] and ligand field calculations [110]. Two approaches have been taken in determining the induced dipole moments, μ^- and μ^+, that appear in equation (13). The induced dipole moments are calculated as the product of its dipole polarizabilities $\alpha^{\pm}$ and the Coulomb field of its counterion. Törring *et al.* [94, 107] derived values $\alpha^{\pm}$ for the alkaline earth monohalides from fitting the ground state dipole moments of the alkali earth monohalides. One objection to this approach is that the resulting effective polarizabilities are unrealistically small compared with those calculated for the free anions. For example, the effective value of $\alpha^-(F^-) = 0.69$ Å^3 [94] was determined from the fit to the alkali halide dipole moments, whereas the *ab initio* prediction gives $\alpha^-(F^-) = 2.61$ Å^3 [111]. Recently, Field and Gittins [112] have proposed an alternative approach for the prediction of the negative

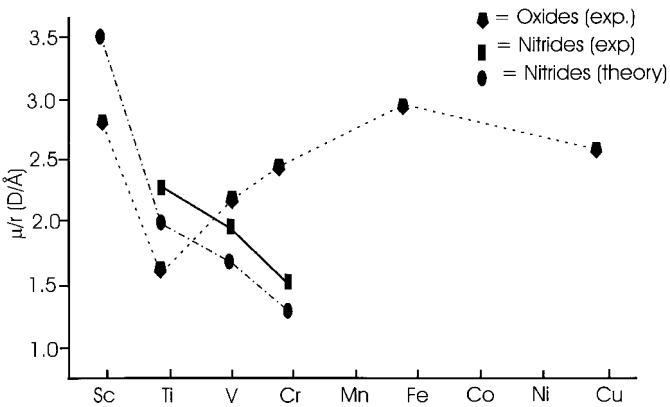

Figure 8. Plot of the experimental values for μ/r_0 for the first row transition metal monoxides and mononitrides.

ion induced dipole moment. They explicitly model the internuclear dependence of μ^- by considering the electric field induced mixing of the ^1S and ^1P electronic states of the anion. In this new approach μ^- exhibits the expected behaviour of remaining finite as the internuclear distance goes to zero (i.e., a saturation effect). Furthermore, this approach removes the mysterious difference between *ab initio* derived values for α^- and the effective values used previously in the Rittner models. With this simple modification to the Rittner polarization model the semi-empirical prediction of μ for the diatomic alkaline earth monohalides is now both quantitative and understandable. Application to the more complicated systems will require the availability of the polarizabilities for anion such as OCH_3^-.

The simple electrostatic polarizability models such as those used for the alkali and alkaline earth monohalides have not been applied widely to transition metal containing radicals. The large number of unpaired electrons and large polarizabilities of the cations for these molecules will make this approach difficult. Although lacking the quantitative predictability of the electrostatic models, a simple molecular orbital (MO) correlation diagram is useful for qualitative predictions of trends in dipole moments, particularly when there are supporting *ab initio* results available. A comparison of the early transition metal mononitrides, ScN, TiN, VN and CrN, is particularly useful because they have been the subject of numerous theoretical predictions. These calculations should be very accurate, given the limited number of valence electrons, moderately low density of low lying states, and the small spin–orbit interaction amongst these states. Although the experiments determine only the magnitude $|\mu|$ of the dipole moment, it is reasonable to expect that the ground and low lying excited state charge distribution is $M^{\delta+}N^{\delta-}$. The value of $|\mu|$ divided by the internuclear distance is a more indicative reflection of the periodic change in bonding because to a first approximation it scales out the geometric dependence. The multireference self-consistent field predictions for μ/r_e by Kunze and Harrison [113, 114] (ScN, 3·58 D Å^{-1}, TiN, 2·05 D Å^{-1}, VN, 1·80 D Å^{-1}, and CrN, 1·235 D Å^{-1}) along with the experimental values for TiN[55], VN[56], CrN[56] and the corresponding experimental values for ScO[48], TiO[53], VO[57] and CrO[58] are plotted in figure 8. The value of μ/r_e for TiN($X^2\Sigma^+$), which is the most thoroughly studied mononitride, varies considerably depending upon the method of calculation. Mattar predicted a value for

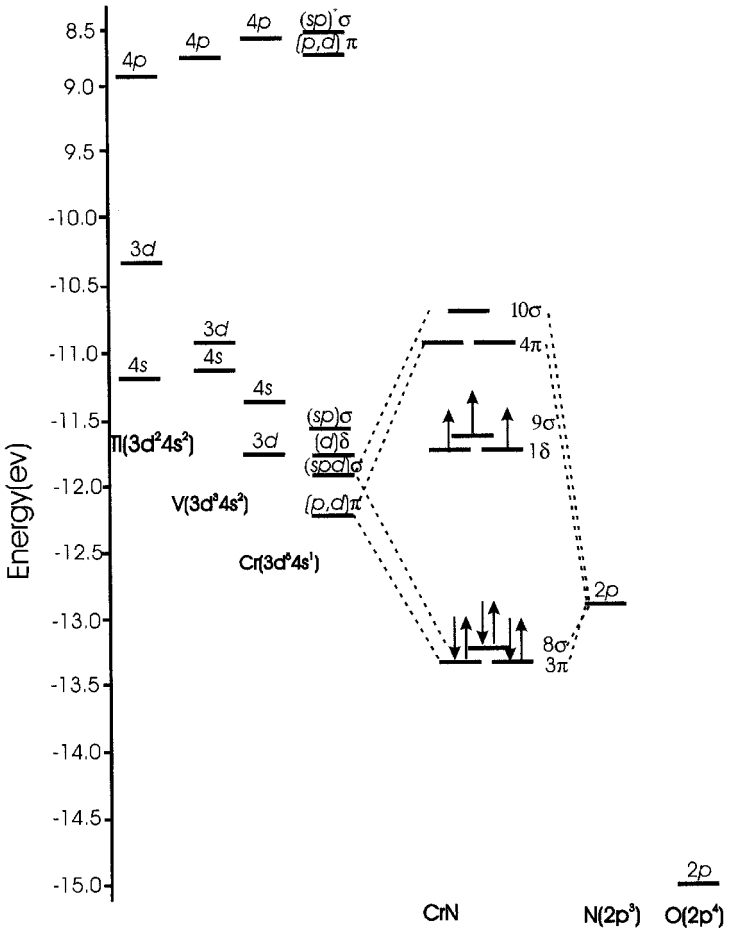

Figure 9. Molecular orbital correlation diagram for CrN. The highest occupied orbital of the metal was assigned an energy which is the weighted mean of the first and second ionization potentials. Upon going from Ti to Cr the 3d orbital rapidly drops in energy, and thus there is a shift of excess N centred charge back to the metal (i.e., enhanced back-bonding in Cr versus Ti).

μ/r_e of 2·33 D Å^{-1} using local density functional theory [115]. Some time ago Bauschlicher predicted a value for μ/r_e of 1·87 D Å^{-1} at the complete active space multireference self-consistent field (CASSCF) level [116], which is in fairly poor agreement with the observed value (2·25 D Å^{-1}) [55].

The simple molecular orbital correlation diagram illustrated in figure 9, which is drawn specifically for CrN, is useful in understanding the trends observed in dipole moments for the mononitrides and monoxides. A plausible ordering of the molecular orbitals for CrN is illustrated in figure 9, which also indicates a ligand induced hybridization of the Cr centred orbitals. The determination of the lowest energy configurations based upon the molecular orbital correlation diagram is complicated by two major considerations. First, the 3d–3d exchange energy is larger than the atomic orbital energy separation. Thus, it may be more advantageous for an electron to occupy a more energetic orbital prior to filling molecular orbitals that have significant 3d contribution. Second, there can be significant changes in the nature and

energy of the molecular orbitals upon excitation. Keeping these limitations in mind it still is valuable to assign primary configurations for the ground states as

$$\text{TiN}: \ldots 8\sigma^2 3\pi^4 9\sigma^1 \rightarrow \text{X}\,^2\Sigma^+,$$
$$\text{VN}: \ldots 8\sigma^2 3\pi^4 9\sigma^1 1\delta^1 \rightarrow \text{X}\,^3\Delta,$$
$$\text{CrN}: \ldots 8\sigma^2 3\pi^4 1\delta^2 9\sigma^1 \rightarrow \text{X}\,^4\Sigma^-.$$

As pointed out by Harrison [114], the trend of decreasing values in the ground state dipole moments on going from TiN to CrN is the result of three competing effects associated with the changes in the 9σ, 8σ and 3π orbitals of figure 9. The 8σ and 3π orbitals are polarized towards the N centre, tending to making a positive contribution to μ, whereas the 9σ orbital is pointed away and has an opposing effect. Upon going from Ti to Cr the 3d orbital rapidly drops in energy and thus there is a shift of excess N centred charge back to the metal (i.e., enhanced back-bonding in Cr versus Ti). This effect contributes to a decrease in $|\mu|$ on going from Ti to Cr. In contrast to the 3d orbital, the energy of the 4s orbital remains much more constant in going from Ti to Cr, and therefore will not, to a first approximation, contribute to the observed decrease of $|\mu|$ on going from Ti to Cr. The larger the hybridization of the back-polarized 9σ orbital the greater the reduction in μ. The propensity for 4s, 4p, 3d hybridization will depend upon the energy separation between the ground $(n-1)\,\text{d}^{x-2}ns^2$ (Ti and V) or $(n-1)\,\text{d}^{x-1}ns^1$ (Cr) configurations and the excited $(n-1)\,\text{d}^{x-2}ns^1np^1$ configuration. This spacing increases on going from Ti to Cr, thus tending to decrease the propensity for 4s–4p hybridization and increase $|\mu|$. Evidently, this increase is not enough to counteract the opposing effect of the 3π polarization. This is basically the same conclusion that Harrison came to from a detailed charge distribution analysis [114].

If simple MO diagrams like that used for the early transition metal mononitrides are to have any utility they should be able to predict qualitatively the differences between the early transition mononitrides and the late transition metal nitrides ReN, IrN, and PtN. Compared with the first row metals the 6s and 5d orbitals are: (a) lower in energy relative to the 2p orbital; (b) have a switched energy ordering (i.e., $E(5\text{d}) < E(6\text{s})$); and (c) have a larger disparity in radial extent. Facets (a) and (b) will tend to make μ/r_e smaller for the third row versus the first row mononitrides because the bonding orbitals will be less polar, whereas (c) will have the opposite effect because the non-bonding σ orbital exhibits less back-polarization. We have measured values of 1·17 D Å^{-1} and 1·03 D Å^{-1} for PtN [89] and IrN [86], respectively, which are smaller than those for TiN, VN and CrN, suggesting that facets (a) and (b) dominate. Although the *ab initio* prediction for PtN was able to reproduce the measured value (μ/r_e(= 1·10 D Å^{-1}) [89]), the data set is too limited for late transition metal set molecules for us to draw any conclusions about their overall quantitative predictability. There are no predictions for IrN or most other third row transition metal diatomic molecules.

5. Concluding remarks

The experimental data set for the permanent electric dipole moments of refractory metal containing molecules has been expanded extensively in the past decade due primarily to developments in the method of production coupled with new spectroscopic techniques. The implementation of optical LIF detection of molecular beam samples have produced values of μ for both the ground and excited electronic states to an accuracy of a few per cent. The data set is primarily restricted to diatomic molecules

with the exception of the alkaline earth monovalent compounds. The alkaline earth monovalent compounds are unique, being easily produced, having high fluorescence quantum yields and generally unperturbed low lying electronic states, conditions not generally found in metal containing polyatomic radicals. Extension of dipole moment determinations to reasonably large polyatomic transition metal containing radicals via the analysis of the Stark effect will require moving into the near-infrared spectral region, where excited state perturbations are expected to be minimized due to the lower density of electronic states. Furthermore, the LIF detection scheme will need to be replaced by a high resolution laser absorption based scheme, because internal conversion and branching of the fluorescence signal into numerous wavelength components will make LIF detection insensitive. Recently we demonstrated that the absorption based near-infrared spectroscopic method of transient frequency modulation has the required sensitivity and resolution for studies of metal containing radicals [117].

Acknowledgements

This work was supported by a grant from the Fundamental Interaction Branch, Division of Basic Energy Sciences, Department of Energy (DE-FG03-94ER14468-004) and the Experimental Chemistry Division of the National Science Foundation (CHE-971074). The author would like to thank Dr. Sidney Golden for his insightful comments.

References

[1] Pauling, L., 1988, *General Chemistry* (New York: Dover).
[2] McWeeney, R., 1979, *Coulson's Valence*, 3rd Edn (Oxford University Press).
[3] Fermi, E., and Teller, E., 1947, *Phys. Rev.*, **72**, 406.
[4] Klahn, Th., and Krebs, P., 1998, *J. chem. Phys.*, **109**, 531.
[5] Debye, P., 1929, *Polar Molecules* (New York: Chemical Catalog Co.).
[6] Onsager, L., 1936, *J. Amer. chem. Soc.*, **58**, 1486.
[7] See for example Luo, Y., Norman, P., and Ågren, H., 1988, *J. chem. Phys.*, **109**, 3589.
[8] Huyskens, P. L., Luck, W. A. P., and Zeegers-Huyskens, T., 1991, *Intermolecular Forces: An Introduction to Modern Methods and Results* (Berlin: Springer-Verlag).
[9] Baldwin, J. E., Goodenough, J. B., Halpern, J., and Rolinson, J. S., 1981, *Intermolecular Forces* (Oxford University Press).
[10] Flygare, W. F., 1978, *Molecular Structure and Dynamics* (Englewood Cliffs, NJ: Prentice-Hall).
[11] Gordy, W., and Cook, R. L., 1984, *Microwave Molecular Spectra* (New York: Wiley).
[12] Townes, C. H., and Schawlow, A. L., 1975, *Microwave Spectroscopy* (New York: Dover).
[13] Bunker, P. R., and Jenson, P., 1998, *Molecular Symmetry and Spectroscopy* (Ottawa: NRC Research Press).
[14] Beuhler, R. J., Berstein, R. B., and Kramer, K. H., 1966, *J. Amer. chem. Soc.*, **88**, 5331.
[15] Brooks, P. R., and Jones, E. M., 1966, *J. chem. Phys.*, **45**, 3449.
[16] Loesch, H. J., and Remschied, A., 1990, *J. chem. Phys.*, **93**, 4779.
[17] Friedrich, B., and Herschbach, D. R., 1991, *Z. Phys. D.*, **18**, 153.
[18] Oudejans, L., Moore, D. T., and Miller, R. E., 1999, *J. chem. Phys.*, **110**, 209.
[19] Loesch, H. J., 1995, *Annu. Rev. phys. Chem.*, **46**, 555.
[20] Freiedrich, B., Slenczka, A., and Herschbach, D., 1995, *Can. J. Phys.*, **72**, 897.
[21] Franks, K. J., Li, H., and Kong, W., 1999, *J. chem. Phys.*, **110**, 11779.
[22] Kawashima, Y., Suenram, R. D., and Hirota, E., 1996, *J. molec. Spectrosc.*, **175**, 99.
[23] Hollowell, C. D., Hebert, A. J., and Street, K., 1964, *J. chem. Phys.*, **41**, 3540.
[24] de Leeuw, F. W., van Wachem, R., and Dymanus, A., 1970, *J. chem. Phys.*, **53**, 981.
[25] Herbert, A. J., Lovas, F., Melendres, C. A., Hollowell, C. D., Story, T. L., and Street, K., 1968, *J. chem. Phys.*, **48**, 2824.

[26] Work in progress at Arizona State University, unpublished.
[27] CEDERBERG, J., OLSON, D., RIOUX, D., DILLEMUTH, T., BOROVSKY, B., LARSON, J., CHEAH, S., CARLSON, M., and STOHLER, M., 1996, *J. chem. Phys.*, **105**, 3361.
[28] VAN WACHEM, R., and DYMANUS, D., 1967, *J. chem. Phys.*, **46**, 3749.
[29] VAN WACHEM, R., DE LEEUW, F. W., and DYMANUS, D., 1967, *J. chem. Phys.*, **47**, 2256.
[30] DE LEEUW, F. W., VAN WACHEM, R., and DYMANUS, D., 1969, *J. chem. Phys.*, **50**, 1393.
[31] STORY JR., T. L., 1968, Thesis, University of California; Lawrence Radiation Laboratory Report UCRL-18484, Berkeley, CA.
[32] TANNIS, M., AUZINSH, M., KLINCARE, I., NIKOLAYEVA, O., FERBER, R., PAZYUK, E. A., STOLYAROV, A. V., and ZAITSEVSKI, A., 1998, *Phys. Rev.* A., **58**, 1932.
[33] CHILDS, W. J., GOODMAN, L. S., NIELSEN, U., and PFEUFFER, V., 1984, *J. chem. Phys.*, **80**, 2283.
[34] ERNST, W. E., and KÄNDLER, J., 1989, *Phys. Rev.* A., **39**, 1575.
[35] ERNST, W. E., and KÄNDLER, J., private communication.
[36] ERNST, W. E., KINDT, S., NAIR, K. P. R., and TÖRRING, T., 1984, *Phys. Rev.* A., **29**, 1158.
[37] ERNST, W. E., and KÄNDLER, J., 1986, *Phys. Rev.* A., **33**, 3588.
[38] KINDT, S., ERNST, W. E., and TÖRRING, T., 1983, *Chem. Phys. Lett.*, **103**, 241.
[39] ERNST, W. E., KÄNDLER, J., LÜDTKE, J., and TÖRRING, T., 1985, *J. chem. Phys.*, **83**, 2744.
[40] STEIMLE, T. C., YUNG, K. Y., FLETCHER, D. A., and SCURLOCK, C. T., 1992, *J. chem. Phys.*, **96**, 2556.
[41] STEIMLE, T. C., FLETCHER, D. A., JUNG, K. Y., and SCURLOCK, C. T., 1992, *J. chem. Phys.*, **97**, 2909.
[42] SCURLOCK, C. T., HENDERSON, T., BOSELY, S., JUNG, K. Y., and STEIMLE, T. C., 1994, *J. chem. Phys.*, **100**, 5481.
[43] MARR, A. J., TANIMOTO, T., GOODRIDGE, D., and STEIMLE, T. C., 1995, *J. chem. Phys.*, **103**, 4466.
[44] PERRY, J., and STEIMLE, T. C., 1995, *J. chem. Phys.*, **103**, 3861.
[45] MARR, A. J., GRIEMAN, F., and STEIMLE, T. C., 1996, *J. chem. Phys.*, **105**, 3930.
[46] NAMIKI, K., ROBINSON, J. S., and STEIMLE, T. C., 1998, *J. chem. Phys.*, **109**, 583.
[47] SIMARD, B., VASSUER, M., and HACKETT, P. A., 1991, *Chem. Phys. Lett.*, **176**, 303.
[48] SHIRLEY, J., SCURLOCK, C., and STEIMLE, T. C., 1990, *J. chem. Phys.*, **93**, 1568.
[49] RICE, S. F., and FIELD, R. W., 1986, *J. molec. Spectrosc.*, **119**, 331.
[50] STEIMLE, T. C., MARR, A. J., and GOODRIDGE, D. M., 1997, *J. chem. Phys.*, **107**, 10406.
[51] STEIMLE, T. C., XIN, J., MARR, A. J., and BEATON, A., 1997, *J. chem. Phys.*, **106**, 9084.
[52] STEIMLE, T. C., SHIRLEY, J. E., SIMARD, B., VASSEUR, M., and HACKETT, P., 1991, *J. chem. Phys.*, **95**, 7179.
[53] STEIMLE, T. C., and SHIRLEY, J. E., 1989, *J. chem. Phys.*, **91**, 8000.
[54] BOUSQUET, R. R., NAMIKI, K., and STEIMLE, T. C., 2000, *J. chem. Phys.*, in the press.
[55] SIMARD, B., NIKI, H., and HACKETT, P. A., 1990, *J. chem. Phys.*, **92**, 7012.
[56] STEIMLE, T. C., ROBINSON, J. S., and GOODRIDGE, D. M., 1999, *J. chem. Phys.*, **110**, 881.
[57] SUENRAM, R. D., FRASER, G. T., LOVAS, F. J., and GILLIES, C. W., 1991, *J. molec. Spectrosc.*, **148**, 114.
[58] STEIMLE, T. C., NACHMAN, D. F., SHIRLEY, J. E., BAUSCHLICHER, C. W., and LANGHOFF, S. R., 1989, *J. chem. Phys.*, **91**, 2049.
[59] STEIMLE, T. C., NACHMAN, D. F., SHIRLEY, J. E., and MERER, A. J., 1989, *J. chem. Phys.*, **90**, 5360.
[60] HOEFT, J., LOVAS, F. J., TIEMANN, E., and TÖRRING, T. T., 1970, *Z. Naturforsch.*, **25a**, 35.
[61] STEIMLE, T. C., NACHMAN, D. F., and FLETCHER, D., 1987, *J. chem. Phys.*, **87**, 5670.
[62] STEIMLE, T. C., CHUNG, W. L., NACHMAN, D. F., and BROWN, J. M., 1988, *J. chem. Phys.*, **89**, 7172.
[63] GRAY, J. A., RICE, S. F., and FIELD, R. W., 1985, *J. chem. Phys.*, **82**, 4717.
[64] HERBT, A. J., LOVAS, F. J., MELENDRES, C. A., HOLLOWELL, C. D., STORY Jr., T. L., and STREET Jr., K., 1968, *J. chem. Phys.*, **48**, 2824.
[65] ERNST, W. E., KÄNDLER, J., KINDT, S., and TÖRRING, T., 1984, *Chem. Phys. Lett.*, **105**, 351.
[66] KÄNDLER, J., MARTELL, T., and ERNST, W. E., 1989, *Chem. Phys. Lett.*, **155**, 470.
[67] KAUFMAN, M., WHARTON, L., and KLEMPERER, W., 1965, *J. chem. Phys.*, **43**, 943.
[68] SHIRLEY, J., SCURLOCK, C., STEIMLE, T. C., SIMARD, B., VASSEUR, M., and HACKETT, P. A., 1990, *J. chem. Phys.*, **93**, 8580.

[69] Bimard, B., James, A. M., and Hackett, P. A., 1992, *J. chem. Phys.*, **96**, 2565.
[70] Simard, B., private communication.
[71] Suenram, R. D., Lovas, F. J., Fraser, G. T., and Matsumura, K., 1990, *J. chem. Phys.*, **92**, 4724.
[72] Steimle, T. C., and Shirley, J. E., 1989, *J. chem. Phys.*, **92**, 3292.
[73] James, A. M., and Simard, B., 1999, *J. chem. Phys.*, **98**, 4422.
[74] Simard, B., Niki, H., and Balfour, W. J., 2000, *J. chem. Phys.*, submitted.
[75] Brugh, D. J., Suenram, R. D., and Stevens, W., 1999, *J. chem. Phys.*, **111**, 3526.
[76] Fletcher, D. A., Dai, D., Steimle, T. C., and Balasubramanian, K., 1993, *J. chem. Phys.*, **99**, 9324.
[77] Fletcher, D. A., Jung, K. Y., and Steimle, T. C., 1993, *J. chem. Phys.*, **99**, 901; 1998, *J. chem. Phys.*, **108**, 10327.
[78] Krisher, L. C., and Norris, W. G., 1966, *J. chem. Phys.*, **44**, 391.
[79] Ernst, W. E., Kändler, J., and Törring, T., 1986, *J. chem. Phys.*, **84**, 4769.
[80] Ernst, W. E., Kändler, J., and Törring, T., 1986, *Chem. Phys. Lett.*, **123**, 243.
[81] Wharton, L., Kaufman, M., and Klemperer, W., 1962, *J. chem. Phys.*, **37**, 621.
[82] Wormsbecher, R., Lane, S. L., and Harris, D. O., 1977, *J. chem. Phys.*, **66**, 2745.
[83] Melanders, C. A., Herbert, A. J., and Street Jr., K., 1969, *J. chem. Phys.*, **51**, 855.
[84] Simard, B., and James, A. M., 1992, *J. chem. Phys.*, **97**, 4669.
[85] Brugh, D., and Suenram, R., private communication.
[86] Marr, A. J., Flores, M. E., and Steimle, T. C., 1996, *J. chem. Phys.*, **104**, 8183.
[87] Steimle, T. C., Jung, K. Y., and Li, B. H., 1995, *J. chem. Phys.*, **102**, 5937.
[88] Beaton, S. A., and Steimle, T. C., 1999, *J. chem. Phys.*, **111**, 10876.
[89] Jung, K. Y., Steimle, T. C., Dai, D., and Balasubramanian, K., 1995, *J. chem. Phys.*, **102**, 643.
[90] Steimle, T. C., Jung, K. Y., and Li, B. H., 1995, *J. chem. Phys.*, **103**, 1767.
[91] Ramsey, N. F., 1956, *Molecular Beams* (Oxford University Press).
[92] Lovas, F. J., and Lide Jr., D. R., 1971, *Advances in High Temperature Chemistry*, Vol. 3, edited by L. Erying (New York: Academic Press) p. 177.
[93] Buckingham, A. D., 1970, *Physical Chemistry; An Advanced Treatise*, Vol. IV, edited by D. Henderson (New York: Academic Press) p. 349.
[94] Törring, T., Ernst, W. E., and Kändler, A. J., 1989, *J. chem. Phys.*, **90**, 4927.
[95] Levenson, M. D., 1982, *Introduction to Nonlinear Laser Spectroscopy* (New York: Academic Press).
[96] Simard, B., Mitchell, S. A., Hendel, L. M., and Hackett, P. A., 1988, *Faraday Discuss. chem. Soc.*, **86**, 163.
[97] Cai, M. F., Miller, T. A., and Bondybey, V. E., 1989, *Chem. Phys. Lett.*, **158**, 475.
[98] Hamrick, Y. M., Taylor, S., and Morse, M. D., 1991, *J. molec. Spectrosc.*, **146**, 273.
[99] Whitham, C. J., Soep, B., Visticot, J.-P., and Keller, A., 1990, *J. chem. Phys.*, **93**, 991.
[100] Buckingham, A. D., 1972, *Physical Chemistry*, *Series One Spectroscopy*, edited by D. A. Ramsey (London: Butterworths), p. 73.
[101] Zare, R. N., 1987, *Angular Momentum: Understanding Spatial Aspects in Chemistry and Physics* (New York: Wiley).
[102] Brown, J. M., Kaise, M., Kerr, C. M. L., and Milton, D. J., 1978, *Molec. Phys.*, **36**, 553.
[103] Lide, D. R., 1998, *CRC Handbook of Chemistry and Physics*, 79th Edn (Boca Raton, FL: CRC Press).
[104] Golden, S., and Wilson, E. B., 1948, *J. chem. Phys.*, **16**, 669.
[105] Bowater, I. C., Brown, J. M., and Carrington, A., 1973, *Proc. R. Soc. Lond.* A, **333**, 265.
[106] Hirota, E., 1985, *High Resolution Spectroscopy of Transient Molecules* (Berlin: Springer-Verlag).
[107] Törring, T., Ernst, W. E., and Kindt, S., 1984, *J. chem. Phys.*, **81**, 4614.
[108] Mestdagh, J. M., and Visticot, J. P., 1991, *Chem. Phys.*, **155**, 78.
[109] Rittner, E., 1951, *J. chem. Phys.*, **19**, 1030.
[110] Rice, S. F., Martin, H., and Field, R. W., 1985, *J. chem. Phys.*, **82**, 5023.
[111] Chong, D. P., and Langhoff, S. R., 1990, *J. chem. Phys.*, **93**, 570.
[112] Field, R. W., and Gittins, C. M., 1997, *J. chem. Phys.*, **106**, 10379.

[113] KUNZE, K. L., and HARRISON, J. F., 1990, *J. Amer. chem. Soc.*, **112**, 3812.
[114] HARRISON, J. F., 1996, *J. chem. Phys.*, **100**, 3513.
[115] MATTAR, S. M., 1993, *J. chem. Phys.*, **97**, 3171.
[116] BAUSCHLICHER, Jr., C. W., 1983, *Chem. Phys. Lett.*, **100**, 51.
[117] STEIMLE, T. C., COSTEN, M. L., HALL, G. E., and SEARS, T. J., 2000, *Chem. Phys. Lett.*, **319**, 363.